ACS SyntheticBiology

pubs.acs.org/synthbio Research Article

Patterning Microtubule Network Organization Reshapes Cell-Like Compartments

Jessica G. Bermudez, Alexander Deiters, and Matthew C. Good*

Cite This: https://doi.org/10.1021/acssynbio.0c00575 Read Online

ACCESS | Metrics & More | Article Recommendations | Supporting Information

ABSTRACT: Eukaryotic cells contain a cytoskeletal network comprised of dynamic microtubule filaments whose spatial organization is highly plastic. Specialized microtubule architectures are optimized for different cell types and remodel with the oscillatory cell cycle. These spatially distinct microtubule networks are thought to arise from the activity and localization of microtubule regulators and motors and are further shaped by physical forces from the cell boundary. Given complexities and redundancies of a living cell, it is challenging to disentangle the separate biochemical and physical contributions to microtubule network organization. Therefore, we sought to develop a minimal cell-like system to manipulate and spatially pattern the organization of cytoskeletal components in real-time, providing an opportunity to build distinct spatial structures and to determine how they are shaped by or reshape cell boundaries. We constructed a system for induced spatial patterning of protein components within cell-sized emulsion compartments and used it to drive microtubule network organization in real-time. We controlled dynamic protein relocalization using small molecules and light and slowed lateral diffusion within the lipid monolayer to create stable micropatterns with focused illumination. By fusing microtubule interacting proteins to optochemical dimerization domains, we directed the spatial organization of microtubule networks. Cortical patterning of polymerizing microtubules leads to symmetry breaking and forces that dramatically reshape the compartment. Our system has applications in cell biology to characterize the contributions of biochemical components and physical boundary conditions to microtubule network organization. Additionally, active shape control has uses in protocell engineering and for augmenting the functionalities of synthetic cells.

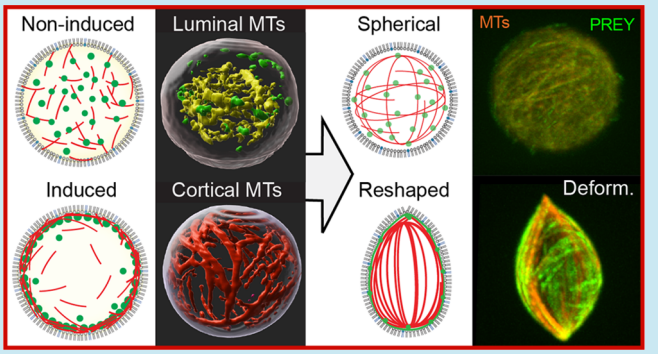

KEYWORDS: *microtubule network, patterned cytoskeleton, minimal cell, boundary conditions, optochemical dimerization, synthetic cell morphology*

INTRODUCTION

Microtubule polymers play an essential role in cell function, including in chromosome segregation, intracellular transport, organelle positioning, and differentiation. The microtubule cytoskeleton is spatially distinct in different cell types, and cells have adapted a variety of strategies to construct and spatially organize the microtubule network. For asymmetric cell divisions, microtubules anchor and bias the position of cell division machinery to direct cytokinesis,[1] which is required for healthy embryo development and renewal of adult tissues. During differentiation of some cell types, microtubules remodel, for example from a central astral array to cortical framework to provide durability to the exterior of differentiated keratinocytes.[2,3] Microtubules also dynamically modulate membrane shape, such as during platelet activation[4] or axon elongation.[5] However, owing to the complexities and redundant systems present in a living cell, it is challenging to dissect the contributions of the positioning and activities of microtubule-associated proteins (MAPS) for regulation of the cytoskeletal architecture.

Microtubule architectures vary among eukaryotic cells, depending on cell type and cell cycle stage. Cytoplasmic microtubules are polarized filaments assembled from α and β tubulin dimers and are highly dynamic. Filament dynamics are controlled by MAPS that bind the ends or walls of the microtubule. Plus-end binders such as End-binding 1 (Eb1) protein and cytoplasmic linker protein (CLIP170) track the dynamic growing or shrinking ends of microtubules.[6,7] MAPs that bind to the wall of the filament, including Tau, play a role in microtubule stabilization, polymerization, and bundling.[8]

Received: November 14, 2020

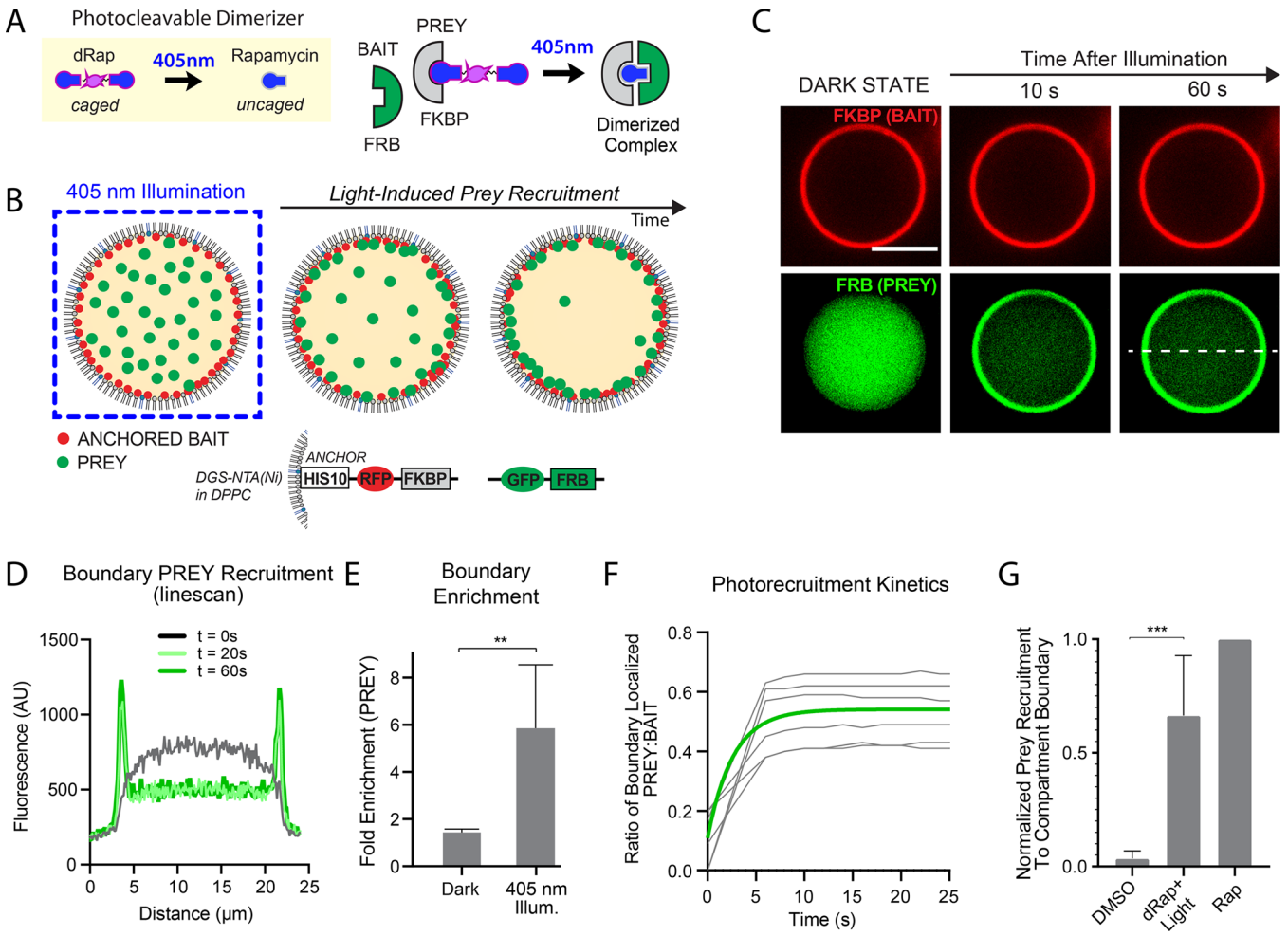

Figure 1. Optochemical dimerization relocalizes a target protein in space and time within a cell-like compartment. (A) Schematic of dRap optochemical dimerization system. (B) Scheme for light-inducible cortical recruitment of GFP−FRB (PREY) system to a His-RFP−FKBP (BAIT) anchored to NTA lipid in the emulsion boundary. (C) Representative confocal microscopy images of rapid GFP−FRB relocalization to the emulsion boundary upon 5 s of 405 nm laser illumination. Aqueous phase contains 2 μM RFP−FKBP, 1.5 μM GFP−FRB, and 1 μM dRap. (D) Representative line scan of the 488 nm channel through widest diameter of emulsion before and after 405 nm illumination. (E) Fold enrichment of GFP−FRB (PREY) at the emulsion boundary in the dark versus illuminated states. $N = 5$. (F) Kinetics of GFP−FRB (PREY) relocalization. Maximum PREY recruitment set relative to fractional recruitment of His-RFP−FKBP (BAIT) to the emulsion boundary. $N = 6$. (G) Quantitation of PREY recruitment to compartment boundary normalized to rapamycin induced dimerization. $N = 6$. dRap uncaging achieves 66.4% of maximum.

Specific regulators of Tau-tubulin interaction, such as the proline-rich region of Tau (TauPRR), and their role in regulating microtubule architecture remain to be explored in depth.[9]

Microtubule networks arise from complex interactions of motor proteins, MAPs, and polymerized tubulin in the cytoplasm, associated with microtubule organizing centers, or anchored to the cell cortex. Simple higher order arrays can be formed by motor proteins and associated complexes such as dynein-dynactin and kinesin.[10,11] Microtubule motors travel along the microtubule or tightly bind to the wall of microtubules when their motor activity is mutated (e.g., dhKinesin).[12]. Astral assemblies of microtubules arise from a localized microtubule organizing center, microtubule bundles, or interactions between microtubules and MAPs, and these are important for control of cell shape, rigidity, and mobility. A cell must tightly regulate the dynamics, stability, and positioning of microtubule networks; mutation of MAPs are associated with several human diseases. Improper regulation of microtubule stability has been linked to neurodegenerative disease,[13] stem cell over proliferation,[14,15] and improper keratinocyte morphogenesis leading to loss of skin barrier function,[2] while faulty expression of spindle positioning factors is linked to errors in cell division and improper cell-fate specification.[16−18]

Separate from microtubule regulatory proteins, the physical dimensions of a cell contribute to the spatial organization of microtubules through confinement.[19] It can often be difficult to distinguish and separate the effects of spatially patterned MAPs from other self-organizing forces in a microtubule network. To address this, a minimal system with cell-like geometry affords the opportunity to build microtubule networks from the ground up, with well-defined biochemical components and confinement conditions. Various microtubule patterns can be generated by manipulating the concentrations of kinesin and cross-linking agent present.[20] Interestingly, microtubule architectures can also be dictated or remodeled by the presence of a physical boundary. Microtubule asters confined in polydimethylsiloxane (PDMS) wells are repositioned and stabilized by the presence of dynein motor protein, demonstrating that physical forces are sufficient to shape the organization of mesoscale microtubule arrays.[21]

https://doi.org/10.1021/acssynbio.0c00575
ACS Synth. Biol. XXXX, XXX, XXX−XXX

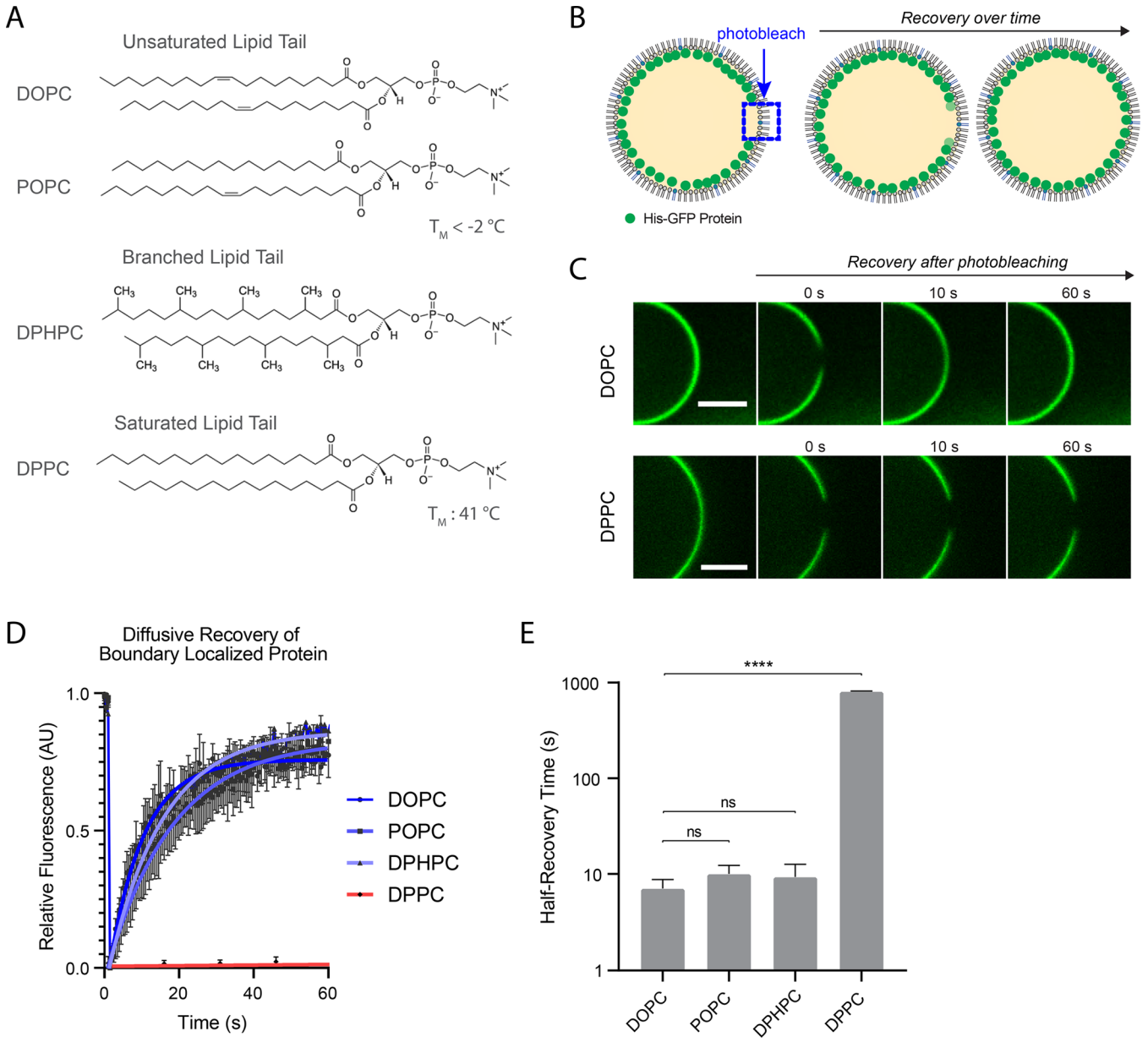

Figure 2. Reduced lipid diffusion enables stable protein anchoring. (A) Chemical composition of branched chain, unsaturated, and saturated lipids tested in Figure 2. (B) Schematic of photobleaching outcomes for His-tagged GFP anchored to DGS-NTA(Ni) in the emulsion boundary. (C) Representative images of His-GFP recovery after photobleaching comparing lipid monolayers composed of DPPC versus DOPC. 3.8% NTA/96.2% DPPC or 3.8 mol % NTA/96.2 mol % DOPC. Aqueous phase contains 1 μM GFP-DHFR. Scale bar = 5 μm. (D) Quantitation of fluorescence recovery for lipid monolayers composed of DPHPC, POPC, DOPC, and DPPC. $N = 3$. (E) Half time of recovery from photobleaching for His-GFP anchored to monolayers of various lipid composition.

The complexity of a living cell often obfuscates the minimal set of components sufficient to drive the organization of microtubule networks. Biochemical studies are necessary to characterize the activities of motors and the collective behavior with MAPs and microtubules, and confinement in microwells, emulsions, and other compartments can be used to approximate the size, shape, and cortical tension of cells. For example, by encapsulating purified microtubules, motors and MAPs, or cell-free cytoplasm in cell-size water-in-oil emulsions or vesicles,[19,22−25] it is possible to mimic a cell-like context. Confinement of microtubule structures in microwells and emulsions has shown that compartment geometry alone can influence microtubule size, orientation, and positioning.[19] When examining the combined effect of biochemical reactions and confinement, the motor protein kinesin-14 can generate either cortical or astral arrangements of microtubules in small and large emulsions respectively.[22]

To understand the dynamic nature of microtubule network reorganization, it is necessary to perturb its organization in real-time. Recent studies using real-time manipulation of microtubules and motor proteins have provided exciting new insights on cytoskeletal network organization.[26] Optogenetic systems such as light-oxygen-voltage 2 (LOV2) have been demonstrated in vivo and optimized in vitro to exhibit 160 μM binding affinity under light conditions.[27,28] In cells, optogenetics tools are useful for altering the local concentration of proteins and recruiting proteins to microtubule ends or the cell boundary.[27−29] A few limitations of these optogenetic tools are that they require

https://doi.org/10.1021/acssynbio.0c00575
ACS Synth. Biol. XXXX, XXX, XXX−XXX

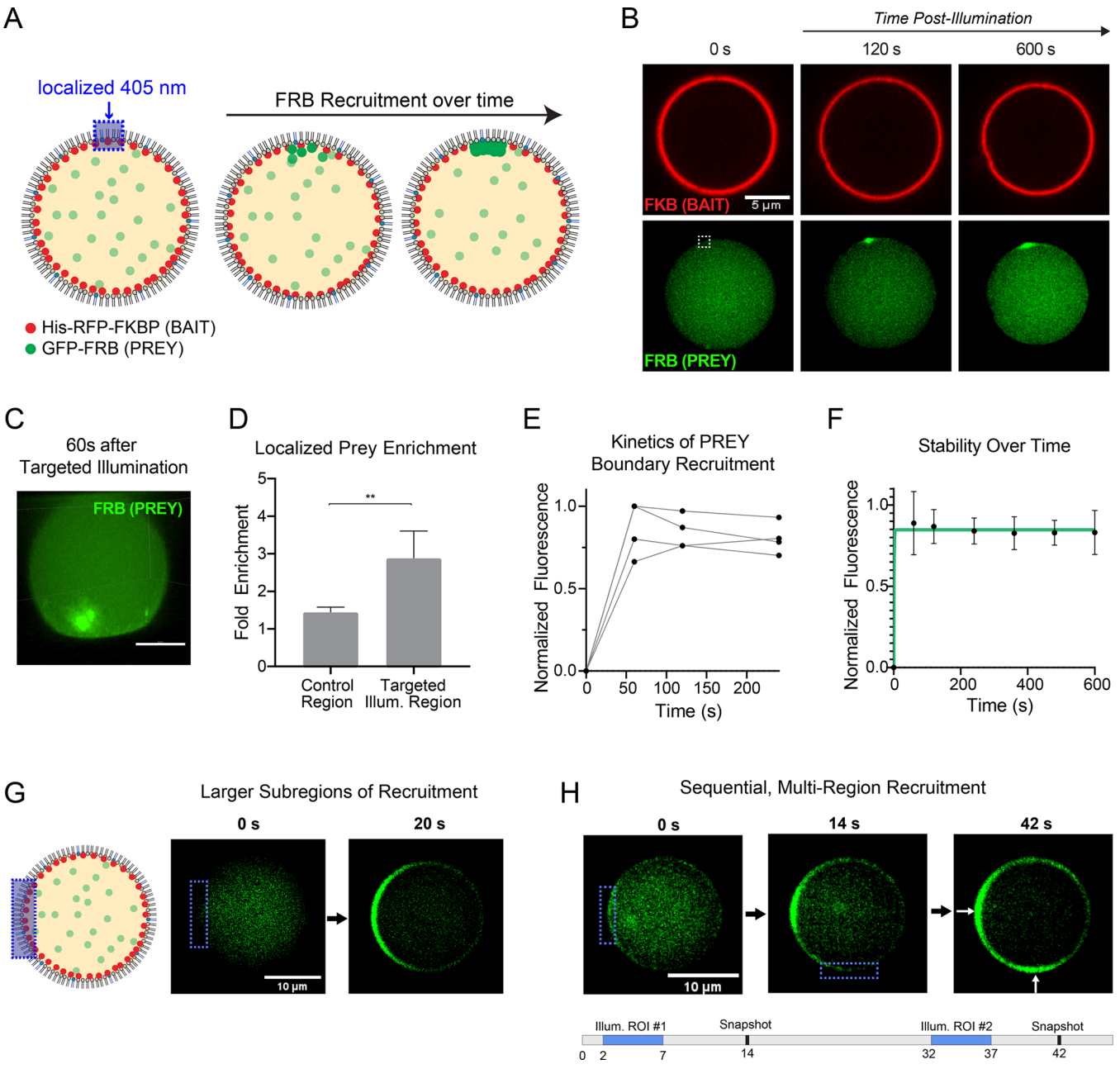

Figure 3. Localized, light-induced micropatterning of a protein to the compartment boundary. (A) Schematic for localized recruitment of GFP−FRB (PREY) to the cortex of the cell-like compartment using focused 405 nm laser. (B) Representative images show localized recruitment of PREY to a micrometer-size spot upon 1 s of illumination with 405 nm ILAS2 laser. (C) Imaris 3D render of localized recruitment of GFP−FRB (PREY) 60 s after targeted illumination. (D) Local fold-enrichment of PREY normalized to the neighboring control region. (E, F) Quantitation of rapid relocalization and stable association of micropatterned GFP−FRB (PREY), relative to His-RFP−FKBP (BAIT), for individual droplets. $N = 3$. Aqueous phase contains 2 μM RFP−FKBP, 1.5 μM GFP−FRB, and 1 μM dRap. (G, H) Photopatterning larger regions of the emulsion boundary. Aqueous phase contains 2 μM RFP−FKBP, 0.75 μM GFP−FRB, and 4 μM dRap. (G) Photopatterned arc of prey recruitment. (H) Sequential two-step recruitment to separate spatial regions of boundary, indicated by white arrows. Schematic of illumination time course.

continuous illumination to maintain dimerization and are difficult to reconstitute in vitro with high light responsiveness. Engineered iLID/SspB does nut fully dimerize in light state without raising components concentrations, which leads to background activation in the dark, off state.[30] Systems such as Pif/PhyB are difficult to activate with light in vitro and require several minutes to dimerize.[31]

Optochemical dimerization tools offer advantages for biochemically reconstituted systems, including high dynamic range of binding in the OFF and ON states and irreversible induction without requiring continuous illumination.[32] By controlling protein−protein interactions using light, it is feasible to manipulate the spatial patterning of components after encapsulation.[31,33] Previously, we demonstrated light-inducible recruitment of proteins from the lumen to the cortex of an emulsion using a photocaged TMP-haloligand dimerizer.[34] Here, we used a photocaged rapamycin (dRap) optochemical system that enables single-pulse irreversible uncaging and protein dimerization (K_D(light) = 12 nM; K_D(dark) = 26 μM).[35] By connecting these tools to microtubule interacting

https://doi.org/10.1021/acssynbio.0c00575
ACS Synth. Biol. XXXX, XXX, XXX−XXX

domains and slowing the lateral diffusion of lipids, we demonstrate spatial reorganization of microtubules within a minimal cell system.

In this study, we built a platform for stable spatial patterning of components within cell-like compartments and used it to remodel microtubule networks in real-time. We anchored a bait protein to create a synthetic cortex and used chemogenetic or optical inputs to trigger cortical relocalization of a protein present in the compartment lumen. To achieve stable photopatterning of protein localization, we slowed lateral diffusion within the lipid monolayer. Additionally, we demonstrated stable protein micropatterning using focused light. To control microtubule network organization, we fused microtubule interacting proteins to the optochemical domains. We demonstrate that induced repositioning of microtubule-interacting proteins reorganizes the spatial structure of microtubule networks. Intriguingly, cortical patterning of polymerizing microtubules breaks network symmetry, and the collective forces dramatically reshape the compartment boundary, reminiscent of the reorganization of the microtubule marginal band in platelets. This system offers a biomimetic platform for cell biology to characterize the contributions of biochemical components and physical boundary conditions to microtubule network organization. Additionally, active shape control has applications in protocell engineering and for the construction of synthetic cells.

RESULTS AND DISCUSSION

Rapid, Light-Inducible Protein Relocalization in Cell-Like Compartments. To spatially pattern protein networks inside a minimal, cell-like system, we implemented the dRap optochemical dimerization system inside water-in-oil emulsions surrounded by a lipid monolayer boundary. A benefit of this optochemical tool is that it uncages in response to just seconds of 405 nm illumination, generating rapamycin that dimerizes the FRB and FKB proteins (Figure 1A).[35] To image the dynamic protein relocalization, we fused FRB to green fluorescent protein (GFP); FKBP was fused to red fluorescent protein (RFP) and a His10 tag that anchors this half of the optochemical pair to a DGS-NTA(Ni) lipid present in the emulsion monolayer (Figure 1B). These recombinant proteins, GFP−FRB ("Prey") and His10−RFP−FKBP ("Bait"), and photocaged dimerizer, dRap, constituted the inner aqueous phase that was encapsulated inside water-in-oil emulsions, stabilized by DOPC lipid in decane in the outer continuous phase. Such cell-size compartments, 10−25 μm in diameter, are highly stable and have been used previously to encapsulate cytoskeletal networks in vitro.[34]

We found that the dRap system was extremely responsive to 405 nm illumination, efficiently and rapidly converting an optical input into a biochemical output. In the dark state, almost no prey was recruited to the emulsion boundary. Upon 5 s of 405 nm illumination, GFP-FRP rapidly was rapidly depleted from the lumen and translocated to His10−RFP−FKBP bait anchored to the lipid monolayer (Figure 1C−D, Figure S1A, Movie S1). After illumination, the boundary enrichment increased from 1.4 to 5.9 (Figure 1E), and the ratio of boundary-localized prey to bait increased to 53% (Figure 1F), whereas the levels of anchored bait (His10−RFP−FKBP) remained constant (Figure S1B). A lower bound for the normalized rate of prey relocalization was minimally 0.3802 s^{-1} (Figure 1F). Such rapid relocalization is orders of magnitude faster than that achieved previously to relocalize large portions of luminal components inside a cell-size compartment.[34] Light-induced recruitment is nearly comparable to the maximum possible relocalization based on pretreatment with constitutive dimerization via rapamycin (Figure 1G, Figure S1C).

Stable Protein Recruitment via Reduced Diffusion in the Lipid Monolayer Boundary. Lipids rapidly diffuse laterally within a lipid bilayer membrane and the lipid monolayer of an emulsion boundary.[36−42] Such rapid diffusion would quickly dissipate any induced spatial patterns of protein recruitment "painted" optically on the compartment boundary. Therefore, we sought to slow the diffusion of DGS-NTA(Ni) lipid within the monolayer boundary by testing various lipids. We characterized a variety of phosphotidylcholine derivatives, including those that are saturated, unsaturated, and contain methylated acyl chains (Figure 2A). Because we were primarily interested in the effects of slowing lipid diffusion on protein anchoring, we measured the dynamics of fluorescent protein recovery from photobleaching (Figure 2B and Movie S2). His10-GFP protein was anchored to 3.8% DGS-NTA(Ni) lipid present in the emulsion monolayer composed of 96.2% candidate lipids. Emulsion boundaries containing DOPC showed very rapid diffusion, reaching 50% recovery from photobleaching within 7 s (Figure 2C−E). Although the methylated acyl chains on DPHPC promote increased lateral interactions among lipid tails in a bilayer,[43] they did little to significantly increase the protein recovery time for anchored GFP (Figure 2E). We next tested a saturated lipid, DPPC, whose gel phase transition temperature is significantly above room temperature. Emulsions stabilized with DPPC displayed half times of recovery from photobleaching of approximately 13 min (Figure 2C−E). Thus, by slowing diffusion within the compartment boundary, we reasoned that stable optical patterning of cytoskeletal networks was feasible.

Localized Photopatterning of Proteins to a Compartment Boundary. To test whether our system would enable real-time spatial control of protein localization, we used a targeted laser to generate polarized patterns of cortical recruitment (Figure 3A). Such a strategy of focusing light can generate micrometer- and submicrometer-size foci of dimerized protein.[31] We encapsulated the recombinant proteins and dRap inside emulsions stabilized by a DPPC lipid monolayer containing DGS-NTA(Ni) lipid. We then optically uncaged dRap within a small region (area = 3 pixels, 0.05 μm^2) of the boundary using targeted laser illumination. Within just a few seconds, we observed localized protein enrichment within a small microdomain (Figures 3B, C, Figure S1D). The prey was locally enriched nearly threefold compared to a neighboring control region that was not illuminated (Figure 3D) and could be patterned quickly, on the order of tens of seconds. Using DPPC in the emulsion monolayer, the localized enrichment of prey protein was sustained over moderately long time scales, decreasing only 15% from the maximum level of enrichment after 10 min (Figures 3E, F). In contrast, when a DOPC monolayer was used and bait protein was diffusible, focused illumination led to only transient localized recruitment. Bait and prey protein quickly diffused around the boundary, dissipating any polarized micropatterns (Figure S1E).

Using focused light to uncage dRap and promote bait−prey dimerization, we achieved multiple types of localized protein patterning to emulsion boundary. In addition to micrometer-size foci, we generated larger patches of recruited prey (Figure 3G). Additionally, we generated multiple distinct patches through sequential focused illumination of spatially distinct boundary regions (Figure 3H). Thus, combining the dRap

https://doi.org/10.1021/acssynbio.0c00575
ACS Synth. Biol. XXXX, XXX, XXX−XXX

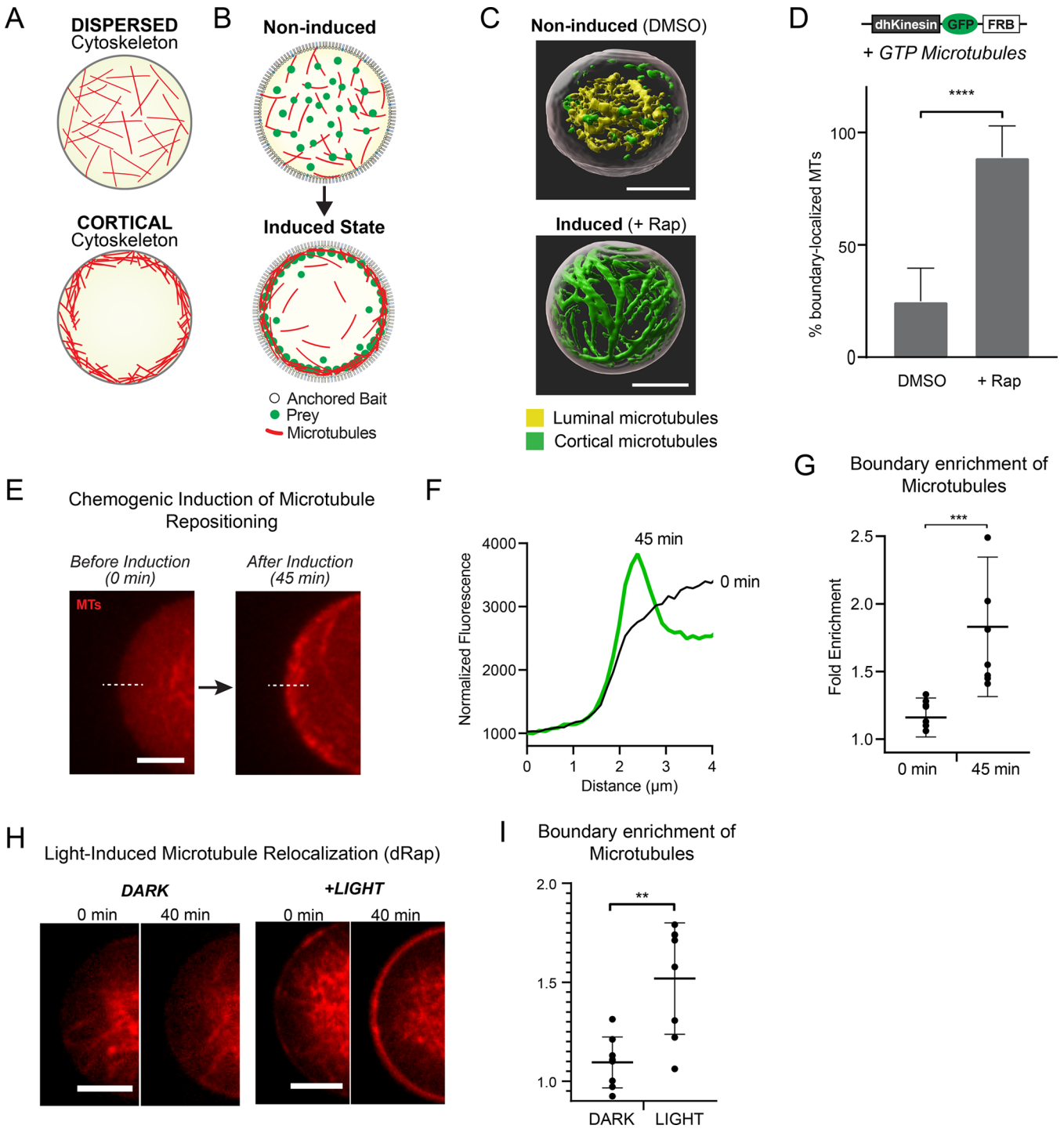

Figure 4. Induced spatial reorganization of microtubules. (A, B) Schematic for inducible relocalization of microtubules from lumen to compartment boundary. (C) Imaris 3D render of GTP microtubules in droplet lumen in absence of dimerizer or anchored to the compartment boundary in the presence of dimerizer. Segmented microtubules: Green: within 0.45 μm of emulsion boundary. Yellow: further than 0.45 μm from the emulsion boundary. Aqueous phase contains 2 μM RFP−FKBP, 300 nM dhKinesin−GFP−FRB, 1 μM dRap, 1 mM GTP, and 60 μM soluble tubulin. (D) Quantification of fraction of GTP microtubules (segmented in Imaris) localized to the compartment boundary in the presence of dhKinesin and rapamycin. $N = 7$. ****P-value $\leq$0.0001. When present, Rap was added to the aqueous phase prior to encapsulation. (E) Representative images of the emulsion boundary before and 45 min after addition of 10 μM rapamycin to the hydrophobic phase after droplets are generated. Scale bar 5 μm. (F) Averaged line scan (2 μm thick) of rhodamine-labeled tubulin across the boundary before and after rapamycin addition. $N = 10$. (G) Quantification of fold enrichment of rhodamine−tubulin at the boundary with rapamycin induction. $N = 10$. ***P-value $\leq$0001. (H) Representative confocal images of light-induced reorganization of the microtubule network before and after in the dark versus 5 s illumination of dRap using the DAPI lamp. Aqueous phase contains 2 μM FKBP, 300 nM dhKinesin−GFP−FRB, 2.5 μM dRap, 1 mM GTP, 1 mM ANPPMP, and 50 μM soluble tubulin. Hydrophobic phase contains 10 mg/mL NTA−POPC in decane. Scale bar 5 μm. (I) Quantification of fold enrichment of rhodamine−tubulin at the compartment boundary in the dark versus 5 s DAPI lamp illumination. $N = 8$ per condition. **P-value $\leq$0.01.

https://doi.org/10.1021/acssynbio.0c00575
ACS Synth. Biol. XXXX, XXX, XXX−XXX

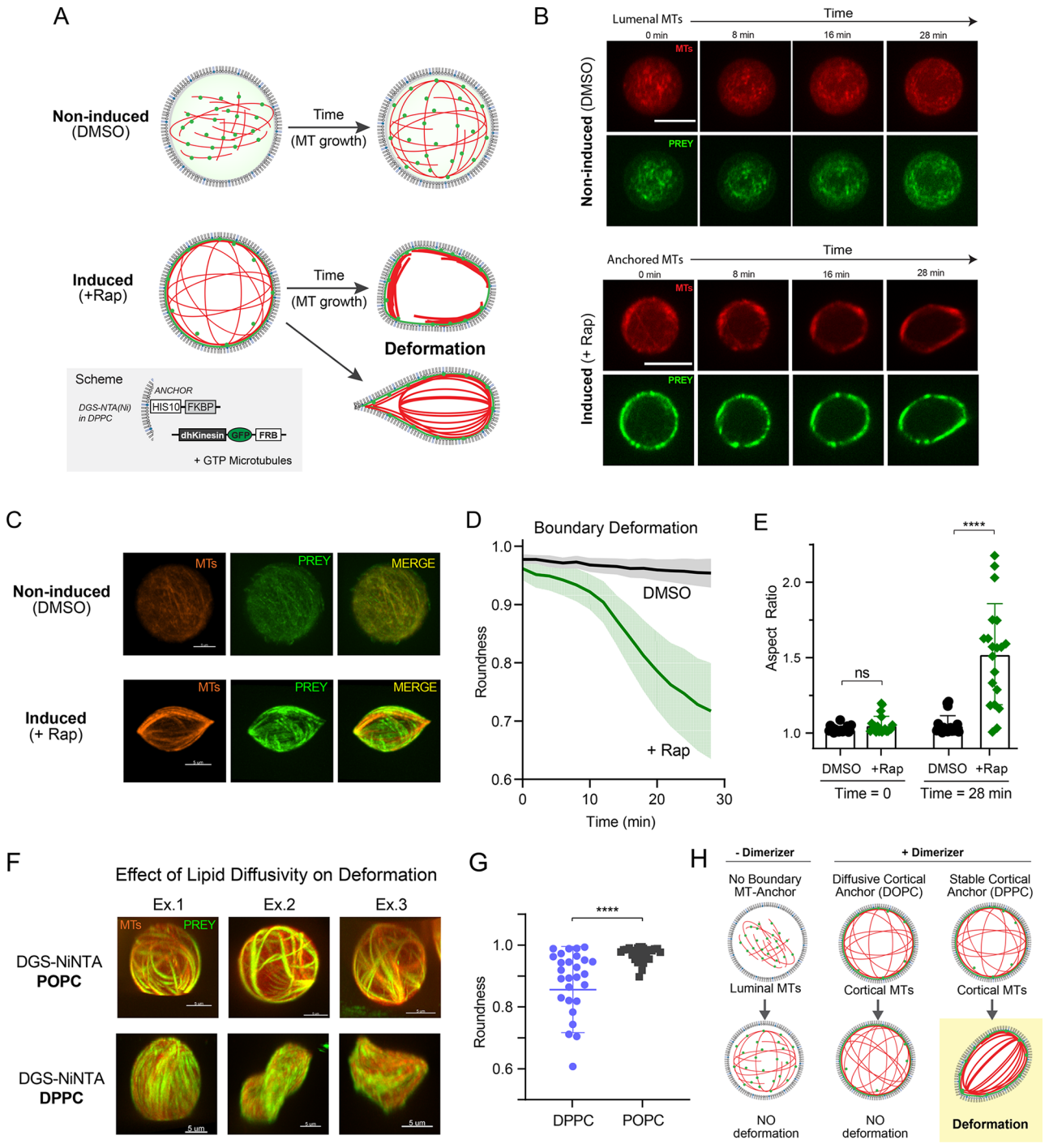

Figure 5. Cortical anchoring of polymerizing microtubules deforms the compartment boundary. (A, B) Schematic of induced cortical recruitment of microtubules and contribution of cortical microtubule polymerization to deformation of the emulsion boundary. (C) Representative images showing emulsion shape after 28 min, comparing no dimerizer control to cortical microtubule array in the presence of dimerizer. Aqueous phase contains 2 μM FKBP, 300 nM dhKinesin−GFP−FRB, 2 μM DMSO or Rap, 1 mM GTP, 1 mM ANPPMP, and 50 μM soluble tubulin. (D) Quantitation of emulsion shape in the presence of DMSO and rapamycin over time; roundness defined as $[4 \times \text{area}]/[\pi \times L_{\text{major axis}}{}^2]$. $N = 20$ per condition. (E) Quantitation of compartment aspect ratio over time. Each data point is an individual emulsion. ****P-value $\leq$0.0001. (F) Representative images showing deformation of emulsion boundaries containing NiNTA−DPPC versus NiNTA−POPC. (G) Quantitation of NiNTA−DPPC and NiNTA−POPC compartment roundness at 16 min. Each data point is an individual emulsion. ****P-value $\leq$0.0001. (H) Schematic: contribution of microtubule localization and stable anchoring to deformation of emulsion compartments.

optochemical dimerization system with a slowly diffusing lipid monolayer inside cell-size emulsions enables rapid optical triggering, relocalization of components from the lumen to cortex, and sustained polarized spatial patterns.

Induced Spatial Reconfiguration of Microtubule Networks. Our goal at the outset of the study was to generate defined spatial patterns of cytoskeletal networks within a minimal cell-like system (Figure 4A). To achieve this, we fused microtubule interacting proteins to our optical dimerizer

https://doi.org/10.1021/acssynbio.0c00575
ACS Synth. Biol. XXXX, XXX, XXX−XXX

bait−prey system inside emulsions loaded with stable or dynamic microtubules (Figure 4B). We selected as candidates a variety of microtubule interacting domains, including those that bind and cluster microtubules, in hopes of spatially partitioning microtubules. We chose domains with tight binding affinities for microtubules, including the proline-rich region of Tau (TauPRR), with an apparent tubulin binding affinity (k_D) of 900 nM,[9] and deadhead Kinesin (dhKinesin), a rigor mutant of kinesin-1,[12] which in its ATP-free form has ∼100 nM affinity for microtubules.[44] We purified recombinant GFP−FRB constructs fused to TauPRR and dhKinesin. As expected, both GFP−FRB−TauPRR and dhKinesin−GFP−FRB coated the surface of GMPCPP and GTP microtubules. To test their functionality at spatially patterning microtubule networks, we encapsulated the microtubule-binding constructs along with microtubules and the His10−FKBP anchor and noncaged rapamycin inside cell-sized emulsions (Figure 4B). We expected that such a strategy would reveal constitutive spatial patterns that could be achieved in our system.

In the absence of binding partners, encapsulated microtubules freely diffuse within a cell-size emulsion or form a central luminal array. We found that when GFP−FRB−TauPRR was recruited to the compartment boundary in the presence of rapamycin, it reproducibly recruited stable GMPCPP microtubules along with it (Figure S2A, B). In the absence of dimerizer, only a small fraction of microtubules interacted with the boundary. Use of a dhKinesin (dhKinesin-GFP−FRB) was even more effective at recruiting microtubules (Figure S2C) and could be paired with longer, dynamic GTP microtubules to generate luminal versus cortex networks (Figure 4C, D and Figure S2D). When anchored by dhKinesin to the compartment boundary, at early time points, these growing microtubules conformed their shape to contours of the emulsion compartment. Importantly, under chemogenic-induced dimerization to localize the microtubule interacting protein to the cortex, more than ∼88% of encapsulated GTP microtubules are recruited to the boundary compared to only 24% in the absence of dimerizer (Figure 4D).

To trigger real-time relocalization of dhKinesin−GFP−FRB, we pipetted 10 μM rapamycin into the hydrophobic lipid and oil phase after the emulsions were formed and observed that microtubules could be inducibly reorganized to the cortex (Figure 4E). Our estimates, based on partitioning coefficient of rapamycin,[45] are that at equilibrium, emulsions would contain approximately 1.7 μM rapamycin, which is sufficient to trigger massive dimerization of bait and prey and relocalization of microtubules. Upon chemogenic-induced relocalization, we observed 1.83-fold enrichment of rhodamine−tubulin fluorescence along the boundary compared to 1.16-fold in noninduced droplets ($p \leq 0.01$) (Figure 4F, G). Similarly, we could induce relocalization of microtubules using light to uncage dRap (Figure 4H). After photoinduction, rhodamine−tubulin fluorescence was enriched ∼1.5-fold at the boundary (Figure 4I). Higher fractional recruitment of microtubules at the cortex upon induction could likely be achieved if our microtubules did not polymerize so quickly, providing a narrow window for triggering. Rapid polymerization after encapsulation leads to an array of microtubules that are no longer freely diffusible, limiting the number that can relocalize to the emulsion boundary. We conclude that inducible recruitment of microtubule-interacting proteins to the cortex is sufficient to spatially reconfigure at least a portion of the minimal tubulin cytoskeleton in cell-size emulsions.

Cortical Tethering of Dynamic Microtubules Deforms Compartment Boundaries. Microtubules grown inside cell-size water-in-oil emulsions whose persistence lengths are larger than the compartment diameter curve around the boundary, and astral arrays conform to size and shape of the compartments due to stiffness of the boundary.[22,46] We wondered whether a polymerizing microtubule array anchored to the cortex rather than localized to the lumen would generate sufficient forces to deform the compartment. We chose a reaction configuration in which dimerizer was included at the outset because this ensured nearly 90% of encapsulated GTP microtubules would localize to the cortex (Figure 4D). Notably, when relocalization was triggered after generating the emulsion compartments, we did not achieve full cortical repositioning of the cytoskeleton, in large part because luminal microtubules grew and some become part of a static array that hindered their induced repositioning.

To determine the functional consequences of growing cortical microtubule arrays, we imaged emulsions containing GTP microtubules and boundary-anchored dhKinesin−GFP−FRB over time, with and without chemogenic anchoring (Figure 5A). Within 10 min of microtubule relocalization, network growth become anisotropic, generating forces that dramatically deformed the normally spherical compartments (Figure 5B). This effect was specific to anchoring microtubules with dhKinesin, as control emulsions lacking bait−prey dimerization did not contain anchored cortical microtubule arrays and did not deform (Figures 5C−E, Movie S3). Comparing emulsions at 28 min, those with induced localization of dhKinesin−GFP−FRB to boundary-anchored bait were much less round (Figure 5D) and had a significantly elevated aspect ratio due to elongation of one or more axes (Figure 5E). Emulsions with boundary-localized dhKinesin−GFP−FRB started visibly deforming at 8 min and reached max deformation around 28 min (Figure 5D, E and Figure S3). Intriguingly, compartment deformation appears to be dependent both on cortical localization of microtubules and stable anchoring (Figure 5H). Deformation was significantly reduced when POPC lipid was used in place of DPPC (Figure 5F, G), suggesting that a diffusive dhKinesin anchor prevents collective force generation. These structural transitions in compartment shape, tied to bundling of a cortical array of microtubules, are reminiscent of the reconfiguration of the marginal band in platelets, where a balance of forces between the cell cortex and microtubule cytoskeleton determine platelet and marginal band shapes.[4,47,48]

CONCLUSIONS

In this study, we present an approach to pattern stable microtubule network architectures inside a cell-size biomimetic system, a novel platform for interrogating regulators of cytoskeletal assembly and for synthetic cell applications. We demonstrate a combined approach to optochemically control protein diffusion and tethering to the minimal cell cortex and slow lipid diffusion to stabilize spatial configurations on a time scale of minutes. By linking optochemical dimerization to microtubule interaction domains, we demonstrate that cortically arrayed and stably anchored GTP microtubules transmit polymerization forces to large-scale deformation of compartment boundaries.

Encapsulation of cytoskeletal components in cell-like geometries reveals the contribution and competition between biochemical interactions and physical forces from the compartment boundary.[22,49,50] In contrast to previous studies that characterized luminal networks and found that emulsion

https://doi.org/10.1021/acssynbio.0c00575
ACS Synth. Biol. XXXX, XXX, XXX−XXX

boundaries can deform reconstituted cytoskeletal polymers, we demonstrated the feasibility of spatial patterning growing microtubules and that cortical positioning of this network is sufficient to deform the interfaces of water-in-oil emulsions. Compartmentalization of nematic networks built from microtubules and motor proteins has illustrated how emergent properties and forces arise from the addition of boundary conditions around enzymatic reactions containing polymer networks.[20,51,52] Here, we demonstrate the converse: that by cortically anchoring microtubule binding proteins in otherwise isotropic compartments, the polymerizing microtubule network will become anisotropic and deform the compartment boundary.

Spatial micropatterning of proteins inside cells and cell-like compartments can be achieved through the embedding of optogenetic or optochemical dimerization domains. A number of excellent optochemical dimerizer systems have been used to pattern proteins on supported lipid bilayers, or to localize proteins to the plasma membrane in cells.[31] Light-regulated anchoring of adaptors for microtubule motors is sufficient to generate pulling forces to orient or relocalize microtubule asters in cells.[53,54] A strength of the optogenetic approach includes reversibility of switching between on and off states using light. However, a challenge of these systems is that they require continuous illumination for stable dimerization in cells and are difficult to implement biochemically in vitro using recombinant proteins. In this study, we built upon an optochemical dimerizer system whose binding constant switches by many orders of magnitude between dark and illuminated states and requires only a short pulse of light to irreversibly control protein interactions.[35] Combining photocaged rapamycin with FRB- and FKBP-tagged microtubule binding domains, we demonstrated chemogenic or optical protein patterning in a synthetic cell-free system. Further, we demonstrated optical patterning of micrometer-size foci and larger patches using targeted illumination.

A challenge that arose in our manipulation of microtubule network organization was ensuring that the network remained dynamic and diffusive throughout the period of time in which to inducibly recruit microtubule-interacting proteins to the boundary. Encapsulated microtubules polymerized quickly, becoming static, thereby reducing the pool of freely available microtubules that can localize to the boundary. In the best case scenario, we included dimerizer in the reaction mix, which led to rapid cortical recruitment of a majority of the microtubules upon formation of the emulsions (Figure 4E). In contrast, when emulsions were formed prior to induced microtubule localization, internal networks assembled in the period of time preceding illumination or chemogenic induction, limiting our ability to relocalize the majority of them. Future studies could improve this system by including photocaged GTP to suppress microtubule growth until spatial patterning of the microtubule binding prey is achieved.

It is intriguing to consider potential physical models to explain how cortically localized GTP microtubules generate sufficient forces to deform the compartment boundary. Water-in-oil emulsions have stiffer boundaries than lipid bilayer vesicles due to high interfacial tension. Surface tension values for water emulsions in a continuous phase of phospholipid and decane are in the range of a few mN/m.[55] Using the law of Laplace, we can estimate the force required to deform the compartment to the aspect ratios observed in Figure 5B. The 10^5 pN of force required would necessitate the collective action tens of thousands of polymerizing microtubule ends. Our images show just upward of dozens of microtubules in a 20 μm diameter emulsion, which suggests that the deformations cannot simply be explained by collective end polymerization forces. There may be additional forces to consider from the effect of crowding proteins on lipid monolayers or bilayers, as others have calculated for vesicles using the Carnahan−Starling equation.[56] Alternatively, large bundles of microtubules with high bending rigidity may contribute to deformation of the lipid monolayer into a lower energy state through the presence of a large number of contact sites with stably anchored dhKinesin.

We propose that these tools and our new platform can be broadly applied to studies of compartmentalized cytoskeletal networks and to formation of force-generating ultrastructures inside synthetic cells. The ability to pattern a cytoskeletal cortex can provide rigidity against compression or generate forces sufficient to reshape the compartment boundaries. The combination of this system with nematic networks could be used to control the direction of symmetry breaking and motility in emulsion systems. Further, these tools could be embedded within cell-free transcription-translation systems to control the partitioning of components inside synthetic compartments. Microtubule networks have been used to partition factors for non-natural amino acid incorporation.[57] We suggest that a similar strategy could be implemented to segregate or colocalize translational components to the boundary of a synthetic compartment.

METHODS

2.1. Molecular Cloning, Protein Expression, and Purification. Constructs were cloned into bacterial expression vectors pRSETa (Thermofisher Scientific) and pETARA.[58] pRSETa was modified to contain an N-terminal 10-Histidine tag. pETARA contains an N-terminal glutathione-S-transferase (GST) fusion tag with a TEV protease cleavable linker. For FRAP assessment of lipid monolayer fluidity, His10-GFP-DHFR was generated by ligation-based cloning of DHFR from pERB260 (a gift from the lab of Michael Lampson, University of Pennsylvania) into His10-GFP vector. For light-inducible relocalization experiments, we generated His10−RFP−FKBP (BAIT) and GST−GFP−FRB (PREY). FKBP and FRB domains were amplified from FRB−WASP and FKBP−Cdc42 (gifted by Michael Rosen, University of Texas, Southwestern) and cloned into modified pRSETa vector containing RFP and a pETARA vector containing GFP, respectively. His10−RFP−FKBP was designed to include a 10-mer disordered linker (GGGGSGGGGS) between RFP and FKBP domains. For microtubule relocalization experiments, GST−GFP−FRB−TauPRR and GST−dhKinesin-GFP−FRB were assembled. Tau was amplified by Phusion (NEB) from a Tau plasmid (gifted by the lab of Elizabeth Rhoades, University of Pennsylvania) and deadhead Kinesin plasmid (gifted by the lab of Yale Goldman Lab, University of Pennsylvania) and assembled into destination plasmids by InFusion cloning (Clontech). All vector constructs were generated in XL1-Blue strains, selected by carbenicillin resistance, and verified by DNA sequencing.

For recombinant protein expression, plasmid constructs were transformed into *E. coli* Rosetta 2 cells (Novagen). Cultures were grown in LB with carbenicillin and chloramphenicol at 37 °C to an OD600 of 0.4, temperature shifted to 16 °C for 25 min, and induced at an OD600 between 0.5 and 0.7 using 0.5 mM

https://doi.org/10.1021/acssynbio.0c00575
ACS Synth. Biol. XXXX, XXX, XXX−XXX

IPTG. Cultures were grown overnight at 16 °C for a total expression time of approximately 20 h.

To purify proteins from cell pellets, cells transformed with His10−GFP−DHFR and His10−RFP−FKBP were resuspended in lysis buffer (150 mM NaCl, 25 mM Tris-pH 7.8, 5% glycerol), lysed with three cycles of sonication and freeze−thaw, repeated twice, and clarified by centrifugation at 16 000 rpm for 20 min. The supernatant was incubated with Ni-NTA agarose superflow resin (Qiagen) for 1 h at 4 °C. After extensive washing, proteins were eluted with NTA elution buffer (500 mM NaCl, 25 mM Tris, 250 mM imidazole pH 8, 10% glycerol). Proteins were dialyzed overnight at 4 °C into a standard protein buffer (150 mM NaCl, 25 mM Tris-pH 7.8, 10% glycerol) for aliquoting and storage. For constructs containing GST-tags, GST−GFP−FRB cultures were resuspended in lysis buffer and GST−GFP−FRB−TauPRR and GST−dhKinesin-GFP−FRB were resuspended in high-salt buffer (500 mM NaCl, 25 mM Tris-pH 7.8, 5% glycerol). All GST-containing cultures were lysed with three cycles of sonication and one cycle of freeze−thaw, repeated twice, and then clarified by centrifugation at 16 000 rpm for 20 min. Supernatants were bound to glutathione agarose resin (Pierce). GST−GFP−FRB and GST−GFP−FRB−TauPRR were eluted with GST elution buffer (15 mM glutathione, 150 mM NaCl, 25 mM Tris-HCl pH 8) and dialyzed overnight at 4 °C into a standard protein buffer. GST−dhKinesin−GFP−FRB was cleaved off-bead by incubating beads with tobacco etch protein (TEV) protease (250 μg TEV protease per mL of beads) in high-salt buffer with 10 mM DTT at RT and further purified by anion exchange (Resource Q) into size exclusion buffer (25 mM Tris, 150 mM NaCl, 10% glycerol). The purity of all purified proteins was verified by sodium dodecyl sulfate-polyacrylamide gel electrophoresis (SDS-PAGE) gels stained with Coomassie before gel imaging. For long-term storage, proteins were supplemented with 2 mM tris(2-carboxyethyl)phosphine (TCEP), flash-frozen, and kept at −80 °C.

2.2. Preparing Water-in-Oil Emulsions. To generate cell-sized emulsions, a hydrophilic phase consisting of soluble proteins in aqueous buffer solution were pipetted in a continuous hydrophobic phase composed of lipids dissolved in decane. Generally, to prepare water-in-oil emulsion, 2.5 μL of an aqueous phase mixture was pipetted up and down to break it apart into smaller droplets within 50 μL of an oil phase, stabilized by a lipid surfactant. To generate the hydrophobic phase, various lipid mixtures in chloroform were dried under a nitrogen stream, placed under vacuum for 4−5 h at room temperature, and then dissolved at 10 mg/mL in decane via 30 min sonication in a 50 °C bath. Undissolved lipid was spun down at 2000 rpm for 11 min. Lipid preparations were purged with nitrogen gas and stored in glass vials sealed with parafilm in a container with dri-rite at temperature of −20 °C. To ensure high activity and low nonspecific binding, lipid mixtures in oil were used for only up to one week after preparation.

For encapsulation of aqueous reaction mixtures, the following conditions were used. For droplet boundary FRAP experiments, 3.8 mol % 1,2-dioleoyl-*sn*-glycero-3-[(N-(5-amino-1-carboxypentyl)iminodiacetic acid)succinyl] (DGS-NTA(Ni)) (Avanti Polar Lipids) was mixed with 96.2 mol % 1-palmitoyl-2-oleoyl-*sn*-glycero-3-phosphocholine (POPC), 1,2-dioleoyl-*sn*-glycero-3-phosphocholine (DOPC), 1,2-dipalmitoyl-*sn*-glycero-3-phosphocholine (DPPC) or 1,2-diphytanoyl-*sn*-glycero-3-phosphocholine (DPHPC), with total lipid mixture at 25 mg/mL in decane. To generate emulsions for FRAP, 2.5 μL of 1 μM His10-GFP-DHFR was diluted in emulsion buffer (25 mM Tris-HCl, 150 mM NaCl, pH 7.8) and encapsulated within 60 μL of each of the four different lipid mixtures. Droplets were transferred to custom acrylic gaskets glued to cover glass for FRAP and imaging. For light-inducible boundary recruitment and microtubule reorganization experiments, emulsions were prepared and imaged as above, except that we used 3.8 mol % DGS-NTA(Ni) and 96.2 mol % DPPC dissolved at 10 mg/mL in decane oil. Hydrophobic phase containing DPPC was preheated in a 50 °C dry bath (above its liquid order transition temperature). Additionally, the quality of all lipids was analyzed for nonspecific interaction with GST−GFP−FRB prey before use.

2.3. Protein Relocalization Experiments, Encapsulated Reaction Mixtures. For light-inducible protein recruitment to the droplet boundary, a 20 μL reaction mixture was prepared containing of 2 μM His10−RFP−FKBP plus DMSO, Rap (Tocris), or dRap and 1.5 μM GFP−FRB in emulsion buffer. His10−RFP−FKBP protein was incubated with equimolar DMSO, Rap, or dRap for 15 min at room temperature to allow binding. Emulsions containing this aqueous reaction mixture were generated by transferring 2.5 μL of the aqueous phase within 50 μL of the NTA-DPPC mixture and repeatedly pipetting until appropriate emulsions sizes were achieved.

2.4. GMPCPP Microtubule Relocalization Experiments, Encapsulated Reaction Mixtures. To generate microtubule seeds for use within emulsions, 1:1000 rhodamine-labeled:unlabeled soluble tubulin was incubated with 1 mM Guanosine-5′-[(α,β)-methyleno]triphosphate (GMPCPP) (Jena Bioscience) in 1× BRB80 buffer (80 mM PIPES, 1 mM $MgCl_2$, 1 mM EGTA, pH 6.8 with KOH) on ice for 5 min. Microtubule mixture was incubated in a 37 °C water bath for 10 min to allow polymerization to occur. Microtubules were spun down at 14 000 rpm for 15 min to remove excess GMPCPP, resuspended in buffer three times, and then resuspended in 30 μL of 1 mM GMPCPP in BRB80 buffer. After incubation of 2 μM His10−RFP−FKBP with DMSO/Rap/dRap for 15 min at room temperature, a reaction mixture was prepared containing 300 nM GFP−FRB−TauPRR or dhKinesin−GFP−FRB, 4% BSA (to minimize nonspecific binding to boundary), and 1 mM GTP; at the last step, 2 μL of 1:10 diluted GMPCPP microtubule suspension was added. Finally, the aqueous reaction mixture was encapsulated within a prewarmed oil mixture (pulled from a 50 °C dry bath) that contained 3.8 mol % DGS-NTA(Ni)/96.2 mol % DPPC dissolved in decane.

2.5. GTP Microtubule Relocalization in Droplets. To generate guanosine triphosphate (GTP) microtubules for de novo polymerization in droplets, 1:1000 rhodamine-labeled:unlabeled soluble tubulin was incubated with 1 mM GTP (Thermofisher) in 1× BRB80 buffer on ice for 5 min. After incubation of 2 μM His10−FKBP with 2 μM DMSO/Rap/dRap, a reaction mixture was prepared with 300 nM dhKinesin−GFP−FRB, 4% BSA (to minimize nonspecific binding to boundary), 1 mM GTP, 1 mM ANPPMP, along with 50 μM tubulin. The mixture was incubated in 50 °C dry bath for 15 s to facilitate later polymerization. The aqueous phase was then encapsulated within a prewarmed oil mixture (pulled from a 50 °C dry bath) that contained 3.8 mol % DGS-NTA(Ni)/96.2 mol % DPPC dissolved in decane.

For chemogenetic induction of microtubule network reorganization, droplets were prepared by mixing 2.5 μL aqueous phase containing 2 μM His10−FKBP−FKBP, 200 nM dhKinesin−GFP−FRB, 2 μM DMSO or Rap, 4% BSA, 1

https://doi.org/10.1021/acssynbio.0c00575
ACS Synth. Biol. XXXX, XXX, XXX−XXX

mM GTP, 1 mM ANPPMP, and 45 μM tubulin (preheated at 50 °C for 10 s) in a 45 μL oil mixture containing DGS-NTA(Ni) lipid and DPPC dissolved in decane. To induce chemogenic microtubule reorganization, we added 10 μM rapamcyin to the oil phase. Based on the logP for rapamycin (4.8, octanol:water), we expected approximately 1.7 μM rapamycin to partition to the aqueous phase. For light-induced microtubule network reorganization, droplets were prepared as for chemogenetic induction, except that 2.5 μM dRap was used in place of Rap, and 50 μM tubulin was used.

2.6. Droplet Deformation Experiments. For droplet deformation and light-inducible microtubule recruitment to the droplet boundary, His10−RFP−FKBP or His10−FKBP (BAIT) was incubated with DMSO (negative control), Rap (noncaged dimerizer), or dRap (photocaged dimerizer) for 15 min at room temperature. Aqueous mixture was prepared using 1.32 μL of bait−dimerizer mixture at ∼15 μM (final concentration: 2 μM bait and 2 μM dimerizer), 300 nM dhKinesin−GFP−FRB, 4% BSA, 1 mM ANPPMP, 50 μM tubulin (1:200 rhodamine-labeled), and 1 mM GTP in BRB80 buffer. Emulsions were generated as described above and transferred to custom gaskets chambers for immediate imaging.

2.7. Illumination and Imaging with Confocal Microscopy. Customized imaging gaskets were prepared by UV-bonding laser cut acrylic and Aquapel-treated glass coverslips using Norland Optical Adhesive. Twenty microliters of water-in-oil emulsion mixture was transferred to custom gaskets for imaging. Emulsions settled to bottom of wells and were imaged using a 100× oil objective via 488 nm (1.29 mW) and 561 nm (1.255 mW) laser illumination on an inverted confocal microscope (Olympus IX81) containing a spinning disk head (Yokogawa X1). Images were acquired using an EM-CCD (Andor iXon3) camera and MetaMorph acquisition software.

Photo-uncaging of dRap was achieved using the following illumination strategies. For widespread uncaging within a field of view at 100× magnification, samples were illuminated with 5 s using the 405 nM laser at 100% intensity (4.14 mW). For targeted photo-uncaging to spatial subregions, we used an iLas2 illuminator system (Roper Scientific) equipped with a 405 nm laser (CrystaLaser LC, model # DL405-050-O). A region of interest for targeted illumination was controlled using the iLas2 software module within MetaMorph. 0% laser power (0.021 mW) and 500 repetitions, totaling 1 s of illumination, were used for local dRap uncaging. Higher laser power led to bleaching.

For cortical light-inducible recruitment, cross-sectional images through the widest region of each droplet were collected once before illumination and every 2 s after illumination. For FRAP experiments in droplets with lipid-disordered lipids, a single cross-sectional image along the widest emulsion plane was collected every 1 s for 30 min, and for liquid-order lipids, every 10 s for 1 min for 8 min. For droplet deformation experiments (Figures 5, S4), cross-sectional images were collected every 2 min for 28 min. Stacks for Figures 3F, 4E, and 5C were collected in both channels at the first and last time points at 0.2 μm intervals.

2.8. Image Analysis. Emulsions were segmented from fluorescence image stacks using ImageJ software. Quantitation was always performed on multiple sets of images and experiments.

For analysis of kinetics of fluorescence recovery, total fluorescence within a photobleached region was measured over time and normalized. Recovery curves were plotted over time and fit using Graphpad Prism software. Half-time to recovery was calculated by fitting a nonlinear one-phase association curve to DOPC, POPC, and DPHPC FRAP curves. For DPPC, half-time to recovery by linear fit and calculating time to half a verage recovery plateau (based on DOPC, POPC, DPHPC data) for DPPC FRAP curves.

For light-inducible protein relocalization via uncaging with widespread 405 nm illumination, partitioning of GFP−FRB (PREY) signal was estimated for the entire volume of the droplet from a single slice through the widest diameter. Percent boundary-localized protein was calculated by dividing total fluorescence in a region within 0.8−1.2 μm from boundary by the total fluorescence in the entire droplet, as described previously.[34] Fold enrichment at the boundary was calculated as the ratio between background-subtracted fluorescence before and after 405 nm illumination.

For localized protein enrichment, several z-stacks were analyzed for each emulsion. Background-subtracted fluorescence at the protein-enriched region was normalized to a neighboring control region along the boundary. Fold enrichment was calculated as the ratio between enriched region and control region.

For microtubule relocalization, the following calculations were performed. For rhodamine-labeled GMPCPP microtubule relocalization, percent of 561 nm fluorescence at the boundary was quantified at 10 min after droplets were formed using the same percent boundary-recruited calculation used for GFP−FRB, as described previously.[34] For analysis of GTP microtubule spatial relocalization, microtubules were segmented using 488 nm in 3D using Bitplane Imaris software with a 0.265 μm Gaussian smoothing filter, 0.3 μm background subtraction, and a threshold of above 285. The emulsion boundary was segmented using a 0.8 μm Gaussian smoothing filter and a threshold of above 340. We defined two populations of microtubules based on their distance from the boundary. Shortest distance calculation was used to label microtubules within 0.75 μm of the droplet boundary as "boundary MTs" and microtubules further than 0.75 μm of the droplet boundary as "luminal MTs". This allowed for recoloring of microtubules based on position.

For emulsion deformation by microtubules, geometries were analyzed as follows. Droplet cross-sectional images were analyzed in ImageJ. Each image was autothresholded using the Triangle method to remove background signal and outline the circumference of the droplet. Roundness and aspect ratio were measured for each slice using Analyze Particle. Roundness is defined as $\frac{4 \times \text{area}}{\pi \times L_{\text{major axis}}^2}$. Aspect ratio is the ratio of the $L_{\text{major axis}}$ to the $L_{\text{minor axis}}$.

2.9. Statistical Analysis. All data was graphed and analyzed for statistical significance in Prism. Unpaired t tests for significance were performed in Prism and depicted on plots with * ($p \leq 0.05$), ** ($p \leq 0.01$), *** ($p \leq 0.001$), **** ($p \leq 0.0001$), or N.S. (not significant).

■ ASSOCIATED CONTENT

Supporting Information

The Supporting Information is available free of charge at https://pubs.acs.org/doi/10.1021/acssynbio.0c00575.

Figure S1, light-induced protein recruitment to compartment cortex; Figure S2, spatial control of microtubule network organization; Figure S3, droplet deformation via cortical tethering of polymerizing microtubules (PDF)

Supplementary Movie 1: rapid, light-induced recruitment of prey protein to the emulsion boundary (AVI)

https://doi.org/10.1021/acssynbio.0c00575
ACS Synth. Biol. XXXX, XXX, XXX−XXX

Supplementary Movie 2: slowed protein diffusion when recruited to a lipid monolayer containing NiNTA-DPPC (AVI)

Supplementary Movie 3: cortical array of polymerizing microtubules deforms compartment boundaries (AVI)

AUTHOR INFORMATION

Corresponding Author

Matthew C. Good − *Bioengineering Graduate Program, Cell and Developmental Biology Department, and Bioengineering Department, University of Pennsylvania, Philadelphia, Pennsylvania 19104, United States;* orcid.org/0000-0002-6367-1034; Email: mattgood@pennmedicine.upenn.edu

Authors

Jessica G. Bermudez − *Bioengineering Graduate Program, University of Pennsylvania, Philadelphia, Pennsylvania 19104, United States;* orcid.org/0000-0001-8622-677X

Alexander Deiters − *Chemistry Department, University of Pittsburgh, Pittsburgh, Pennsylvania 15260, United States;* orcid.org/0000-0003-0234-9209

Complete contact information is available at: https://pubs.acs.org/10.1021/acssynbio.0c00575

Author Contributions

J.G.B. and M.C.G. conceptualized the project and designed experiments. A.D. designed and synthesized the dRap molecule. J.G.B. performed the experiments. J.G.B. and M.C.G. analyzed data. J.G.B. and M.C.G. wrote the manuscript; A.D. revised the text. M.C.G. and A.D. secured funding for the project.

Notes

The authors declare no competing financial interest.

ACKNOWLEDGMENTS

We thank Elizabeth Rhoades and Yale Goldman for providing constructs encoding microtubule interacting proteins, the Katya Grishchuk lab and Wangxi Luo for technical guidance on microtubule reconstitution, and Andrea Stout and the CDB Microscopy core for imaging support. We thank Daniel Hammer for calculations of the forces required for filaments to deform compartment boundaries. Funding to support this research included a Cell and Molecular Biology Training Grant from the National Institutes of Health (5-T32-GM007229-39) (J.G.B.) and a Fontaine Fellowship (J.G.B.). Additionally, the work was supported by a CASI grant from the Burroughs Wellcome Fund (M.C.G.), a New Investigator Grant from the Charles E. Kaufman Foundation (M.C.G.), a McCabe Fund Fellow Award (M.C.G.), and a National Science Foundation (NSF) iSuperseed grant, DMR1720530 (M.C.G.). Synthesis of optochemical dimerizers was supported by NSF grant CHE-1404836.

ABBREVIATIONS

Rap, rapamycin; dRap, photocaged dimerized rapamycin; GTP, guanosine triphosphate; GMPCPP, nonhydrolyzable GTP

REFERENCES

(1) Kaltschmidt, J. A., and Brand, A. H. (2002) Asymmetric cell division: microtubule dynamics and spindle asymmetry. *Journal of Cell Science*, 2257−2264.

(2) Muroyama, A., and Lechler, T. (2017) Microtubule organization, dynamics and functions in differentiated cells. *Development 144*, 3012−3021.

(3) Lechler, T., and Fuchs, E. (2007) Desmoplakin: an unexpected regulator of microtubule organization in the epidermis. *J. Cell Biol. 176*, 147−154.

(4) Cuenca-Zamora, E. J., Ferrer-Marin, F., Rivera, J., and Teruel-Montoya, R. (2019) Tubulin in Platelets: When the Shape Matters. *Int. J. Mol. Sci. 20*, 3484.

(5) Reinsch, S. S., Mitchison, T. J., and Kirschner, M. (1991) Microtubule polymer assembly and transport during axonal elongation. *J. Cell Biol. 115*, 365−379.

(6) Wieczorek, M., Bechstedt, S., Chaaban, S., and Brouhard, G. J. (2015) Microtubule-associated proteins control the kinetics of microtubule nucleation. *Nat. Cell Biol. 17*, 907−916.

(7) Dhonukshe, P., and Gadella, T. W., Jr. (2003) Alteration of microtubule dynamic instability during preprophase band formation revealed by yellow fluorescent protein-CLIP170 microtubule plus-end labeling. *Plant Cell 15*, 597−611.

(8) Hernandez-Vega, A., Braun, M., Scharrel, L., Jahnel, M., Wegmann, S., Hyman, B. T., Alberti, S., Diez, S., and Hyman, A. A. (2017) Local Nucleation of Microtubule Bundles through Tubulin Concentration into a Condensed Tau Phase. *Cell Rep. 20*, 2304−2312.

(9) McKibben, K. M., and Rhoades, E. (2019) Independent tubulin binding and polymerization by the proline-rich region of Tau is regulated by Tau's N-terminal domain. *J. Biol. Chem. 294*, 19381−19394.

(10) Tan, R., Foster, P. J., Needleman, D. J., and McKenney, R. J. (2018) Cooperative Accumulation of Dynein-Dynactin at Microtubule Minus-Ends Drives Microtubule Network Reorganization. *Dev. Cell 44*, 233−247.

(11) Ross, T. D., Lee, H. J., Qu, Z., Banks, R. A., Phillips, R., and Thomson, M. (2019) Controlling organization and forces in active matter through optically defined boundaries. *Nature 572*, 224−229.

(12) Nakata, T., and Hirokawa, N. (1995) Point Mutation of Adenosine Triphosphate-binding Motif Generated Rigor Kinesin That Selectively Blocks Anterograde Lysosome Membrane Transport. *J. Cell Biol. 131*, 1039−1053.

(13) Cappelletti, G., Surrey, T., and Maci, R. (2005) The parkinsonism producing neurotoxin MPP+ affects microtubule dynamics by acting as a destabilising factor. *FEBS Lett. 579*, 4781−4786.

(14) Wang, H., Somers, G. W., Bashirullah, A., Heberlein, U., Yu, F., and Chia, W. (2006) Aurora-A acts as a tumor suppressor and regulates self-renewal of Drosophila neuroblasts. *Genes Dev. 20*, 3453−3463.

(15) Lee, C. Y., Andersen, R. O., Cabernard, C., Manning, L., Tran, K. D., Lanskey, M. J., Bashirullah, A., and Doe, C. Q. (2006) Drosophila Aurora-A kinase inhibits neuroblast self-renewal by regulating aPKC/Numb cortical polarity and spindle orientation. *Genes Dev. 20*, 3464−3474.

(16) Izumi, Y., Ohta, N., Hisata, K., Raabe, T., and Matsuzaki, F. (2006) Drosophila Pins-binding protein Mud regulates spindle-polarity coupling and centrosome organization. *Nat. Cell Biol. 8*, 586−593.

(17) Bowman, S. K., Neumuller, R. A., Novatchkova, M., Du, Q., and Knoblich, J. A. (2006) The Drosophila NuMA Homolog Mud regulates spindle orientation in asymmetric cell division. *Dev. Cell 10*, 731−742.

(18) Siller, K. H., Cabernard, C., and Doe, C. Q. (2006) The NuMA-related Mud protein binds Pins and regulates spindle orientation in Drosophila neuroblasts. *Nat. Cell Biol. 8*, 594−600.

(19) Pinot, M., Chesnel, F., Kubiak, J. Z., Arnal, I., Nedelec, F. J., and Gueroui, Z. (2009) Effects of confinement on the self-organization of microtubules and motors. *Curr. Biol. 19*, 954−960.

(20) Roostalu, J., Rickman, J., Thomas, C., Nedelec, F., and Surrey, T. (2018) Determinants of Polar versus Nematic Organization in Networks of Dynamic Microtubules and Mitotic Motors. *Cell 175*, 796−808.

(21) Kerssemakers, J. W., Munteanu, E. L., Laan, L., Noetzel, T. L., Janson, M. E., and Dogterom, M. (2006) Assembly dynamics of microtubules at molecular resolution. *Nature 442*, 709−712.

(22) Baumann, H., and Surrey, T. (2014) Motor-mediated cortical versus astral microtubule organization in lipid-monolayered droplets. *J. Biol. Chem. 289*, 22524−22535.
(23) Good, M. C., Vahey, M. D., Skandarajah, A., Fletcher, D. A., and Heald, R. (2013) Cytoplasmic Volume Modulates Spindle Size During Embryogenesis. *Science 342*, 856.
(24) Abu Shah, E., and Keren, K. (2014) Symmetry breaking in reconstituted actin cortices. *eLife 3*, No. e01433.
(25) Jimenez, A. M., Roche, M., Pinot, M., Panizza, P., Courbin, L., and Gueroui, Z. (2011) Towards high throughput production of artificial egg oocytes using microfluidics. *Lab Chip 11*, 429−434.
(26) Tas, R. P., Chen, C. Y., Katrukha, E. A., Vleugel, M., Kok, M., Dogterom, M., Akhmanova, A., and Kapitein, L. C. (2018) Guided by Light: Optical Control of Microtubule Gliding Assays. *Nano Lett. 18*, 7524−7528.
(27) Guntas, G., Hallett, R. A., Zimmerman, S. P., Williams, T., Yumerefendi, H., Bear, J. E., and Kuhlman, B. (2015) Engineering an improved light-induced dimer (iLID) for controlling the localization and activity of signaling proteins. *Proc. Natl. Acad. Sci. U. S. A. 112*, 112−117.
(28) Strickland, D., Lin, Y., Wagner, E., Hope, C. M., Zayner, J., Antoniou, C., Sosnick, T. R., Weiss, E. L., and Glotzer, M. (2012) TULIPs: tunable, light-controlled interacting protein tags for cell biology. *Nat. Methods 9*, 379−384.
(29) Adikes, R. C., Hallett, R. A., Saway, B. F., Kuhlman, B., and Slep, K. C. (2018) Control of microtubule dynamics using an optogenetic microtubule plus end-F-actin cross-linker. *J. Cell Biol. 217*, 779−793.
(30) Hallett, R. A., Zimmerman, S. P., Yumerefendi, H., Bear, J. E., and Kuhlman, B. (2016) Correlating in Vitro and in Vivo Activities of Light-Inducible Dimers: A Cellular Optogenetics Guide. *ACS Synth. Biol. 5*, 53−64.
(31) Jia, H., Kai, L., Heymann, M., Garcia-Soriano, D. A., Hartel, T., and Schwille, P. (2018) Light-Induced Printing of Protein Structures on Membranes in Vitro. *Nano Lett. 18*, 7133−7140.
(32) Klewer, L., and Wu, Y. W. (2019) Light-Induced Dimerization Approaches to Control Cellular Processes. *Chem. - Eur. J. 25*, 12452−12463.
(33) Bartelt, S. M., Chervyachkova, E., Steinkuhler, J., Ricken, J., Wieneke, R., Tampe, R., Dimova, R., and Wegner, S. V. (2018) Dynamic blue light-switchable protein patterns on giant unilamellar vesicles. *Chem. Commun. (Cambridge, U. K.) 54*, 948−951.
(34) Caldwell, R. M., Bermudez, J. G., Thai, D., Aonbangkhen, C., Schuster, B. S., Courtney, T., Deiters, A., Hammer, D. A., Chenoweth, D. M., and Good, M. C. (2018) Optochemical Control of Protein Localization and Activity within Cell-like Compartments. *Biochemistry 57*, 2590−2596.
(35) Brown, K. A., Zou, Y., Shirvanyants, D., Zhang, J., Samanta, S., Mantravadi, P. K., Dokholyan, N. V., and Deiters, A. (2015) Light-cleavable rapamycin dimer as an optical trigger for protein dimerization. *Chem. Commun. (Cambridge, U. K.) 51*, 5702−5705.
(36) Block, S. (2018) Brownian Motion at Lipid Membranes: A Comparison of Hydrodynamic Models Describing and Experiments Quantifying Diffusion within Lipid Bilayers. *Biomolecules 8*, 30.
(37) Di Rienzo, C., Gratton, E., Beltram, F., and Cardarelli, F. (2013) Fast spatiotemporal correlation spectroscopy to determine protein lateral diffusion laws in live cell membranes. *Proc. Natl. Acad. Sci. U. S. A. 110*, 12307−12312.
(38) Eggeling, C., Ringemann, C., Medda, R., Schwarzmann, G., Sandhoff, K., Polyakova, S., Belov, V. N., Hein, B., von Middendorff, C., Schonle, A., and Hell, S. W. (2009) Direct observation of the nanoscale dynamics of membrane lipids in a living cell. *Nature 457*, 1159−1162.
(39) Jan Akhunzada, M., D'Autilia, F., Chandramouli, B., Bhattacharjee, N., Catte, A., Di Rienzo, R., Cardarelli, F., and Brancato, G. (2019) Interplay between lipid lateral diffusion, dye concentration and membrane permeability unveiled by a combined spectroscopic and computational study of a model lipid bilayer. *Sci. Rep. 9*, 1508.
(40) Khmelinskaia, A., Mucksch, J., Conci, F., Chwastek, G., and Schwille, P. (2018) FCS Analysis of Protein Mobility on Lipid Monolayers. *Biophys. J. 114*, 2444−2454.
(41) Kusumi, A., Shirai, Y. M., Koyama-Honda, I., Suzuki, K. G., and Fujiwara, T. K. (2010) Hierarchical organization of the plasma membrane: investigations by single-molecule tracking vs. fluorescence correlation spectroscopy. *FEBS Lett. 584*, 1814−1823.
(42) Machan, R., and Hof, M. (2010) Lipid diffusion in planar membranes investigated by fluorescence correlation spectroscopy. *Biochim. Biophys. Acta, Biomembr. 1798*, 1377−1391.
(43) Shinoda, W., Shinoda, K., Baba, T., and Mikami, M. (2005) Molecular Dynamics Study of Bipolar Tetraether Lipid Membranes. *Biophys. J. 89*, 3195−3202.
(44) Crevel, I. M.-T. C., Lockhart, A., and Cross, R. A. (1996) Weak and Strong States of Kinesin and ncd. *J. Mol. Biol. 257*, 66−76.
(45) Information, N. C. f. B. (2021) PubChem Compound Summary for CID 5284616, Sirolimus.
(46) Juniper, M. P. N., Weiss, M., Platzman, I., Spatz, J. P., and Surrey, T. (2018) Spherical network contraction forms microtubule asters in confinement. *Soft Matter 14*, 901−909.
(47) Thon, J. N., Macleod, H., Begonja, A. J., Zhu, J., Lee, K. C., Mogilner, A., Hartwig, J. H., and Italiano, J. E., Jr. (2012) Microtubule and cortical forces determine platelet size during vascular platelet production. *Nat. Commun. 3*, 852.
(48) Dmitrieff, S., Alsina, A., Mathur, A., and Nedelec, F. J. (2017) Balance of microtubule stiffness and cortical tension determines the size of blood cells with marginal band across species. *Proc. Natl. Acad. Sci. U. S. A. 114*, 4418−4423.
(49) Opathalage, A., Norton, M. M., Juniper, M. P. N., Langeslay, B., Aghvami, S. A., Fraden, S., and Dogic, Z. (2019) Self-organized dynamics and the transition to turbulence of confined active nematics. *Proc. Natl. Acad. Sci. U. S. A. 116*, 4788−4797.
(50) Fanalista, F., Birnie, A., Maan, R., Burla, F., Charles, K., Pawlik, G., Deshpande, S., Koenderink, G. H., Dogterom, M., and Dekker, C. (2019) Shape and Size Control of Artificial Cells for Bottom-Up Biology. *ACS Nano 13*, 5439−5450.
(51) Sanchez, T., Chen, D. T., DeCamp, S. J., Heymann, M., and Dogic, Z. (2012) Spontaneous motion in hierarchically assembled active matter. *Nature 491*, 431−434.
(52) Deek, J., Maan, R., Loiseau, E., and Bausch, A. R. (2018) Reconstitution of composite actin and keratin networks in vesicles. *Soft Matter 14*, 1897−1902.
(53) Okumura, M., Natsume, T., Kanemaki, M. T., and Kiyomitsu, T. (2018) Dynein-Dynactin-NuMA clusters generate cortical spindle-pulling forces as a multi-arm ensemble, *eLife 7* DOI: 10.7554/eLife.36559
(54) Fielmich, L.-E., Schmidt, R., Dickinson, D. J., Goldstein, B., Akhmanova, A., and Van den Heuvel, S. (2018) Optogenetic dissection of mitotic spindle positioning in vivo. *eLife 7* DOI: 10.7554/eLife.38198
(55) Venkatesan, G. A., Lee, J., Farimani, A. B., Heiranian, M., Collier, C. P., Aluru, N. R., and Sarles, S. A. (2015) Adsorption Kinetics Dictate Monolayer Self-Assembly for Both Lipid-In and Lipid-Out Approaches to Droplet Interface Bilayer Formation. *Langmuir 31*, 12883−12893.
(56) Stachowiak, J. C., Schmid, E. M., Ryan, C. J., Ann, H. S., Sasaki, D. Y., Sherman, M. B., Geissler, P. L., Fletcher, D. A., and Hayden, C. C. (2012) Membrane bending by protein-protein crowding. *Nat. Cell Biol. 14*, 944−949.
(57) Reinkemeier, C. D., Girona, G. E., and Lemke, E. A. (2019) Designer membraneless organelles enable codon reassignment of selected mRNAs in eukaryotes. *Science 363*, eaaw2644.
(58) Bhattacharyya, R. P., Remenyi, A., Good, M. C., Bashor, C. J., Falick, A. M., and Lim, W. A. (2006) The Ste5 scaffold allosterically modulates signaling output of the yeast mating pathway. *Science 311*, 822−826.

https://doi.org/10.1021/acssynbio.0c00575
ACS Synth. Biol. XXXX, XXX, XXX−XXX